Modified hydrotalcites as chloride scavengers and inhibitor release agents for improved corrosion protection of reinforced concrete

Zhengxian Yang [1], Rob Polder [2,3], J.M.C. Mol [4]

[1] College of Civil Engineering Fuzhou University, Fuzhou, Fujian 350116, China
[2] Section of Materials and Environment, Faculty of Civil Engineering and Geosciences, Delft University of Technology, P.O. Box 5048, 2600 GA Delft, the Netherlands
[3] TNO Structural Reliability, P.O. Box 155, 2600 AD Delft, the Netherlands
[4] Department of Materials Science and Engineering, Faculty of Mechanical, Maritime and Materials Engineering (3mE), Delft University of Technology, Mekelweg 2, 2628 CD Delft, the Netherlands

Owing to the unique molecular structure and high ion exchange capacity, hydrotalcites are believed to have a potential to be modified and tailor-made as an active corrosion protective component of reinforced concrete. In this paper, two types of modified hydrotalcites (MHT-pAB and MHT-NO_2) were tested both in alkaline solution and mortar for their possibilities as chloride scavengers and inhibitor release agents for application in concrete. The test in alkaline solution showed that ion exchange occurred between free chloride ions in solution and the intercalated inhibitive anions in the MHTs. The results in mortar validated that MHTs could be promising alternatives for preventing chloride-induced corrosion when an appropriate dosage is adopted and applied in a proper way, in particular, either incorporation of a certain amount (MHT-pAB to replace 5% weight of cement) in the bulk mortar or as a coating of the reinforcing steel (MHT-pAB or MHT-NO_2 at 20% weight of cement).

Keywords: Modified hydrotalcites, chloride, concrete, corrosion, inhibitors

1 Introduction

An essential feature in the long term durability of a reinforced concrete structure is the protection of the steel reinforcement. Under normal conditions, steel in concrete is

protected from corrosion by a passive layer that is formed due to the high alkalinity of the concrete pore solution. However, the passive layer can be destroyed and corrosion initiated by certain aggressive species at the steel surface which may penetrate through the concrete cover (Bertolini et al. 2013). Among the aggressive species, chloride is the most detrimental and abundant culprit and has been recognized as one of the major factors affecting the service life of reinforced concrete structures (Polder and Peelen 2002, Yang et al. 2009, Polder et al. 2012). As proposed by Tuutti (Tuutti 1982), the development of corrosion in reinforced concrete consists of two different stages. The first stage (i.e., initiation phase) is related to the penetration of chloride up to the critical concentration to the surface of the reinforcement. The second stage (i.e., propagation phase) is related to actual reinforcement corrosion, steel bar cross section loss, concrete cover cracking and spalling, compromising serviceability and eventually, structural safety. Therefore, the best corrosion prevention strategy may need to include two aspects: 1) to slow down chloride transport in concrete, e.g. by improving the chloride binding capacity of the concrete which subsequently would result in delayed corrosion initiation of the reinforcing steel; 2) to slow down the corrosion propagation after corrosion has initiated, which would result in a longer time before concrete is damaged and steel section loss has undesired consequences. Most traditionally available corrosion prevention approaches such as coatings on reinforcing steel, concrete surface sealers, stainless steel reinforcement and cathodic prevention (Cigna et al. 2002, Elsener et al. 2010, Elsener 2001, Pedeferri 1996, Polder et al. 2016) focus on one of the aspects and less attention has accordingly been paid to the other. A promising option is adding modified hydrotalcites to concrete as an alternative approach against chloride ingress into concrete (Yang et al. 2013, Yang et al. 2014, Yang et al. 2015). Hydrotalcite is one representative of a large mineral group of Layered Double Hydroxides (LDHs), in general formula $[M^{II}_{1-x}\ M^{III}_{x}(OH)_2]^{x+}\ [(A^{n-}_{x/n})]^{x-} \cdot mH_2O$, where M^{II} and M^{III} are di- and trivalent metals respectively and A^{n-} is an exchangeable interlayer anion with valence n. The x value is in the range of 0.22-0.33. Hydrotalcites are poorly soluble (micro)crystalline solids. Common metals in hydrotalcites are Mg (II) and Al (III), but many other metal atoms can be present including Ca and Fe. The anions A^{n-} are loosely bound and can be exchanged for any other anion in the surrounding solution. Many naturally occurring hydrotalcites contain carbonate anions. LDH family members are for example ettringite, which is based on Ca, Al and sulphate; and Friedl's salt, based on Ca, Al and chloride. When a particular anion is intentionally intercalated during synthesis, the resulting compound is called a modified

hydrotalcite, MHT. A typical structure of LDHs is schematically shown in Figure 1 (Yang et al. 2013). Due to the unique characteristic of the molecular structure and high anionic exchange capacity, hydrotalcite is believed to have a potential to be modified or tailor-made as an active component of concrete.

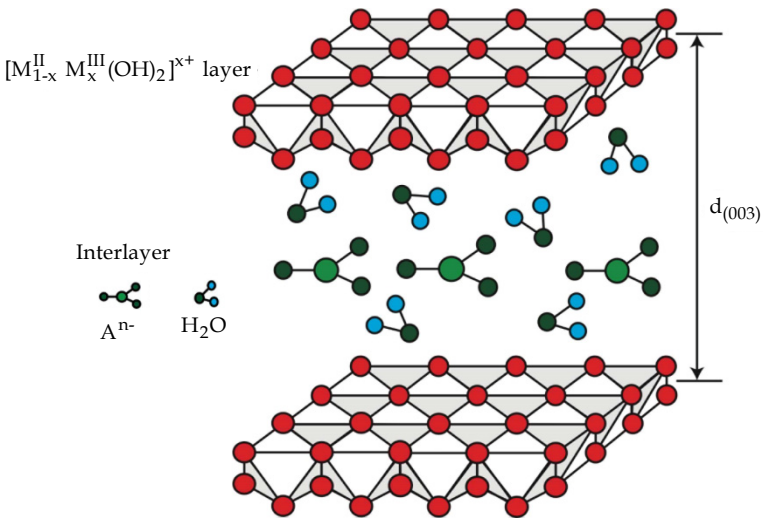

*Figure 1. Schematic representation of a typical LDH molecular structure (*d*-spacing value* $d_{(003)}$ *is the length of the interlayer space; adapted from (Yang et al. 2013)).*

Hydrotalcite has been found in hydrated blast furnace slag cements, which are known to bind more chloride ions than pure Portland cements (Dhir et al.1996, Arya and Xu 1995, Glass and Buenfeld 2000). More recently, Kayali et al. (Kayali et al. 2012) demonstrated the remarkable role of hydrotalcite in chloride binding and corrosion protection in concretes with blast furnace slag. If inhibitive anions are intercalated into MHT's, it may be expected that chloride ions in the pore solution will be bound, simultaneously releasing the inhibitive anions. Consequently, such a MHT may have a dual function working mechanism: capturing aggressive chlorides and simultaneously releasing inhibitive interlayer anions (Yang et al. 2013). Both effects can be simplified in the following schematic chemical reaction:

$$\text{MHT-In} + Cl^- \rightarrow \text{MHT-Cl} + In^- \quad (1)$$

with MHT-In a hydrotalcite with intercalated inhibitive anion In^- (in the matrix), MHT-Cl the hydrotalcite with chloride intercalated and In^- the inhibitive anion in the pore solution.

This paper presents an overview of the research into modified hydrotalcites as chloride scavengers and inhibitor release agents for concrete application and their effect on corrosion initiation in mortar.

2 Materials and methods

2.1 ***Materials***

Two types of MHTs denoted as MHT-pAB and MHT-NO_2 were used in this study. They were synthesized by the modification of Mg(2)Al-CO_3 (with "2" in parentheses showing that the atomic ratio of Mg/Al is 2:1) with sodium p-aminobenzoate (-pAB) and sodium nitrite (-NO_2) respectively through a calcination-rehydration procedure (Yang et al. 2013a). Elemental analysis showed that 11% NO_2- and 32% -pAB by mass of corresponding MHT had been incorporated into their molecular structures. The hydrotalcite (Mg(2)Al-CO_3) was a commercially available product PURAL® MG 63 HT provided by Sasol Germany GmbH.

CEM I 42.5N cement, CEN-Standard sand (particle size 0-2 mm) and deionized water were used for preparing mortar specimens. Reinforcing steel was low-carbon steel (B500A, ribbed) bars with a nominal diameter of 8 mm. The relevant electrode materials for mortar tests are: AISI 304 type stainless steel mesh with a wire thickness of 0.5 mm and mesh width of 1.6 mm, platinized titanium mesh with a wire thickness of 1.2 mm and mesh width of about 2 mm, copper plate with a thickness of 0.8 mm, and REF401 type (Radiometer Analytical) Saturated Calomel Electrode (SCE).

2.2 ***Test in alkaline solutions***

The chloride binding and inhibitor releasing properties of the two MHTs were investigated in a mixed solution containing 0.1 M NaOH and 0.5 M NaCl to simulate the concrete pore solution strongly contaminated by chlorides. For this test, a volume of 20 ml solution of 0.1 M NaOH and 0.5 M NaCl was vigorously mixed with 0.5 g powder of MHTs in a screw capped glass centrifuge tube. The suspension was then sealed to isolate it from the atmosphere and put in a rotating device at room temperature for a predetermined period of exchange time to allow the occurrence of ion exchange. The ion exchange time was set at 2 h, 6 h, 12 h, 24 h, 48 h, 72 h, 96 h and 120 h. Afterwards, the remaining solid at each exchange time point was separated from bulk solution by centrifugation and then washed thoroughly with deionized water. The separated solid was collected and oven dried for 24 h at 105 ^{o}C under vacuum. Then, the chlorides in the solid as well as the inhibitors released

through the ion exchange in the supernatant were analyzed photometrically using a Spectroquant® NOVA 60 spectrophotometer. Duplicates were measured simultaneously to ensure the reliability of the test results. In addition, X-ray powder diffraction (XRD) was employed to further validate whether or not the ion exchange reaction indeed occurred between MHTs and chlorides.

2.3 ***Test in mortars***

2.3.1 Sample preparation

Pre-treatment of the reinforcing steel bars

Steel bars were cut into 120 mm long pieces from a longer bar. The newly cut ends were slightly ground to remove sharp edges. Before being embedded in mortar, the bars were pretreated to remove any rust to get a uniform surface condition using a chemical cleaner solution (1:1 diluted HCl + 3 g/l urotropine).

Mortar with embedded reinforcing steel

MHT was incorporated in two different ways: (1) as one of the mixing components in mortar; (2) as part of cement paste coating of the reinforcing steel. For (1), the mortar samples were prepared with a constant (cement + MHT) content, a constant water-to-(cement + MHT) mass ratio of 0.50, a constant sand-to-(cement + MHT) mass ratio of 3 and MHT-to-(cement + MHT) mass percentages of 0%, 5%, 10%, respectively. In fact, MHT was used to replace cement. This means the "true" water-cement (w/c) ratio was 0.50, 0.53 and 0.56 respectively for the three replacement levels. For (2), a cement paste was pre-mixed with a water-to-cement ratio of 0.40 (without MHT) or a water-to-(cement + MHT) mass ratio of 0.4 and MHT to replace 20% cement mass. Then the cement paste was uniformly applied over the surface of the steel bars with approx. 1.5-2.0 mm thickness as shown in Figure 2. The coated bars were subsequently stored in a fog room and cured for 24 h before being embedded into mortar (without MHT).

As shown in Figure 3, mortar specimens were prisms of 40 × 40 × 110 mm^3 in which a 120 mm long steel bar was embedded at a cover depth of 10 mm. The bar was isolated from the air/mortar interface using insulating heat shrink tubing. The geometric length and surface area of the steel bar that were exposed to mortar were 60 mm and 1560 mm^2 respectively.

Eight groups of mortar specimens were prepared:

1) Bar in mortar without addition of MHT (Ref.);
2) Bar coated with pure cement paste and without addition of MHT in mortar (Ref. (coating));
3) Bar in mortar with 5% replacement of MHT-pAB (MHT-pAB (5%));
4) Bar in mortar with 10% replacement of MHT-pAB (MHT-pAB (10%));
5) Bar coated with cement paste containing MHT-pAB and without addition in mortar (MHT-pAB(coating));
6) Bar in mortar with 5% replacement of MHT-NO_2 (MHT-NO_2 (5%));
7) Bar in mortar with 10% replacement of MHT-NO_2 (MHT-NO_2 (10%));
8) Bar coated with cement paste containing MHT-NO_2 and without addition in mortar (MHT-NO_2 (coating)).

Figure 2. Freshly coated steel bars (left) and coated bars (right) after being cured for 24 hours in a fog room

The mortar prisms were cast in molds and sealed by plastic film. The detailed mixing procedure can be found in our previous study (Yang et al. 2015), in which the MHT's effect on the properties of fresh and hardened mortar were reported. They were demolded 24 h after casting and moved to a fog room. The specimens were taken out of the fog room at 28 days. After wiping off excess water, a PVC-pond (about 50 mm in depth) was glued to the top surface of the specimens. All vertical surfaces of the mortar specimens were carefully

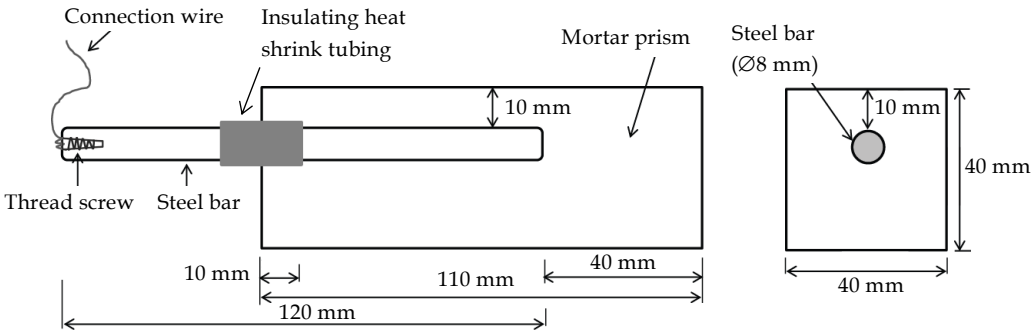

Figure 3. Schematic illustration of reinforced mortar specimen

coated with silicone sealant to prevent water evaporation during the test. When the silicone sealant had completely hardened after 24 h, the specimens were transferred to a plastic tray, in which tap water was added in order to keep the bottom surface of the specimens in a wet condition. The PVC-ponds of the specimens were filled with a saturated $Ca(OH)_2$ solution and covered by plastic film for 3 days to prevent drying. Then the $Ca(OH)_2$ solution was removed and the PVC-ponds were rinsed using tap water before being filled by the chloride solution.

2.3.2 Anti-corrosion performance evaluation

In this study, a modified accelerated migration test based on Andrade's integral corrosion test (Andrade and Rebolledo 2012, Castellote et al. 2002, Andrade and Buják 2013) was employed to evaluate the anti-corrosion performance of two MHTs. This test was conducted by exposure of mortar specimens to accelerated ingress of chloride until corrosion initiation; occurrence of corrosion initiation was based on open circuit potential (OCP) and linear polarization resistance (LPR) measurements.

The principle of the accelerated chloride migration test is to apply an external electrical potential across the mortar specimen forcing the chloride ions to migrate into the specimen. Figure 4 schematically illustrates the electrode arrangement and cross-sectional view of a mortar specimen. The copper plate acting as cathode was submerged in chloride solution, while a stainless steel mesh acting as anode was placed underneath the specimen. The stainless steel mesh was also used as the counter electrode (CE) when LPR measurement was performed. A water-saturated sponge was sandwiched between the stainless steel mesh and the specimen to ensure good electrical contact. A potential drop of

6 V was applied between copper cathode and stainless steel anode in order to accelerate the migration of the chloride ions through mortar towards the embedded rebar. The ponding solution was a solution of 0.6 M NaCl and 0.4 M $CuCl_2$. The reason for choosing $CuCl_2$ is that the dominant cathodic reaction will be $Cu^{2+} + 2\ e \rightarrow Cu$. The advantage is that it does not produce hydroxyl ions, which might alter the transport of chloride ions in the mortar.

OCP and LPR measurements

OCP and LPR measurements were carried out using a Solartron analytical SI1287 potentiostat coupled with an eight-channel 1281 multiplexer. As can be seen from Figure 4, a two reference electrode system was adopted for OCP measurement. RE1, i.e., a Saturated Calomel Electrode (SCE) was used for manually measuring the OCP, while the platinized titanium mesh (RE2) was used as another reference electrode for automatically measuring the OCP through the custom designed computer program. A conventional three-electrode electrochemical system was employed for LPR measurements with the steel bar as working

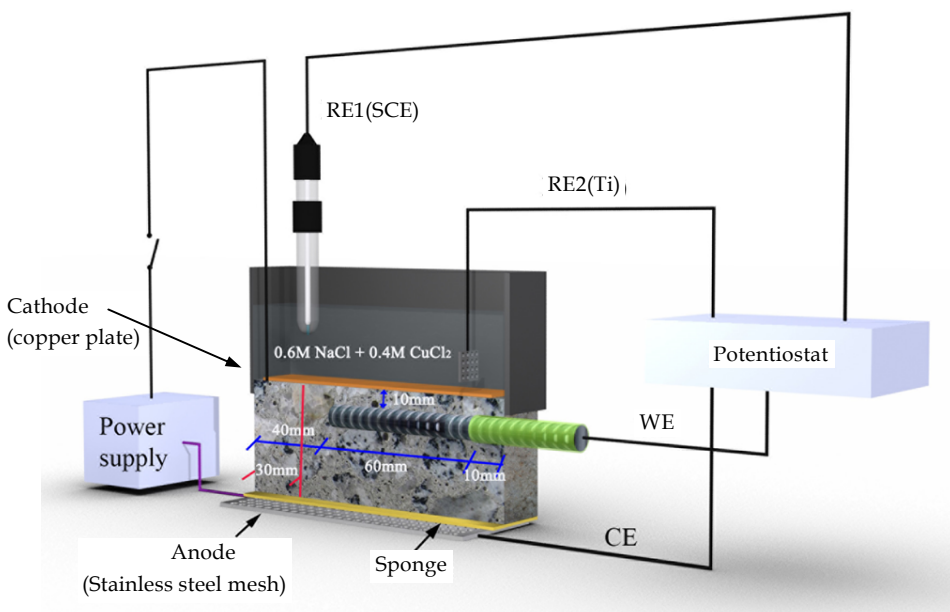

Figure 4. Schematic cross-sectional view of the experimental setup for accelerated chloride migration test. WE (working electrode): Reinforcing steel bar; CE (counter electrode): Stainless steel mesh used as the Anode with the copper plate as the Cathode; RE1 (reference electrode 1): Saturated calomel electrode (SCE); RE2 (reference electrode 2): Platinized titanium mesh.

electrode (WE), the stainless steel mesh as the counter electrode (CE) and the platinized titanium mesh (RE2) as the reference electrode.

When a certain voltage is applied to a reinforced mortar/concrete specimen, polarization of the reinforcing steel occurs even if the steel is not connected to the power source. This polarization may in turn cause the passive film on the reinforcing steel to become unstable and (more) vulnerable to be destroyed upon the arrival of chloride ions. In order to study such a polarization effect, pre-tests were performed by applying 6 V potential to a reinforced mortar specimen by a power supply. The polarization effect was measured by switching off the power for 45 – 90 minutes and monitoring the potential change. The results of the pre-tests suggested that the OCP and LPR measurements could be done in a near-natural condition with limited polarization effects. Therefore, in the real experiments, the OCP was manually recorded versus SCE, two or three times per day, after a 45-90 min waiting period as well as automatically recorded versus RE2 three times per day after waiting for 90 min. The LPR was measured once per day upon finishing the OCP measurements, 90 min after switching off the power.

Prior studies have shown that the OCP (i.e. corrosion potential, E_{corr}) can provide qualitative information on the probability of corrosion (Poursaee and Hansson 2007, Baweja et al.1993) and is usually employed to indicate the occurrence of depassivation (i.e., corrosion initiation). However, the indication from OCP might lead to misunderstanding in some cases either because the potential shift may not be detected or because it may not really account for a significant activity. Such uncertainties promote the need for use of the corrosion current as an additional parameter. The corrosion current (I_{corr}) can be calculated from the polarization resistance (R_p) obtained by LPR measurement according to the Stern-Geary equation (Eq. 2)

$$I_{corr} = \frac{B}{R_p} \tag{2}$$

where B is a proportionality constant and a typical value of 26 mV is normally used for active corrosion and 52 mV for passive steel in concrete (Andrade and Gonzalez 1978). I_{corr} is often expressed as corrosion current density (i_{corr}) when the surface area of the steel is taken into account. In this study, observable shifts in the evolution of E_{corr} as well as i_{corr} over time were set as criteria to identify the moment of the depassivation of the embedded steel bars. As a quantitative measure for shifting criteria, the empirical

boundary values of E_{corr} = -350 mV (SCE) and i_{corr} = 0.1 µA/cm² were adopted (Andrade and Buják 2013, Alonso et al. 2000). This is: if E_{corr} is found to be more negative than -350 mV and/or i_{corr} higher than 0.1 µA/cm², it can be considered that corrosion has been initiated and active corrosion is developing. For OCP measurement using the platinized titanium mesh (Ti, RE2) as the reference electrode, however no well-established boundary value of E_{corr} is applicable and the results were viewed as additional information to OCPs measured by SCE. For simplicity, the results of LPR measurements are not reported here; for more details on those, refer to (Yang 2015).

Once depassivation was detected, the specimens were taken out of the experimental setup. Then, different procedures were followed for MHT in bulk application and coating application. For specimens in which MHT was incorporated as a mortar mixing component (bulk), a 30 mm slice was cut off from the side of mortar prism without rebar (see Figure 5A). This 30 mm mortar slice was used for chloride threshold (CT) analysis as will be discussed below. The newly cut surface of the mortar prism was immediately sealed using Bison® silicone kit and the pond on the top of the prism was re-glued in which chloride solution was refilled. The mortar prism was then placed back in the experimental setup in order to continuously monitor the corrosion process after depassivation without applying a potential until around 30 days. For specimens in which MHT was applied as coating of the rebar, two specimens were broken upon their individual depassivation from which CT at the rebar depth was analyzed. The other three or four specimens were left for continued monitoring of the corrosion process after depassivation without applying a potential.

Chloride analysis

After depassivation and dismantling, the chloride content at rebar depth was analyzed to investigate the effect of MHT on the CT.

Sampling: Depending on the way that MHT was applied, different sampling methods were employed. As shown in Figure. 5A, for specimens in which MHT was incorporated in mortar bulk (App. #1, bulk), a 30 mm slice was cut off from the mortar prism for CT analysis. This 30 mm slice was thought to have the same chloride penetration depth as that in the main part of the mortar prism near the rebar (Polder and Peelen 2002). In this way, the main part of the prism could be kept for continued monitoring the corrosion process after corrosion initiation. For CT analysis, a small amount of mortar powder (about 2 g) at

the rebar depth (7.5-12.5 mm) was collected by dry drilling (drill diameter: 5 mm) from the 15 mm thick part of the 30 mm slice that was originally close to the rebar. Considering that in the "coating" specimens the material composition at the interfacial zone of the embedded steel bar (the cement paste coating containing MHT) is different from the rest of the mortar (without MHT), the specimens in which MHTs were applied as coating of the rebar (App. #2, coating) were broken upon depassivation and mortar powder (about 2 g) was drilled directly from the interfacial zone of the rebar surface at the depth of 7.5-12.5 mm (Figure 5B).

Analysis: The total (acid-soluble) chloride contents of the mortar powders were analyzed photometrically using a Spectroquant® NOVA 60 photometer following the procedure

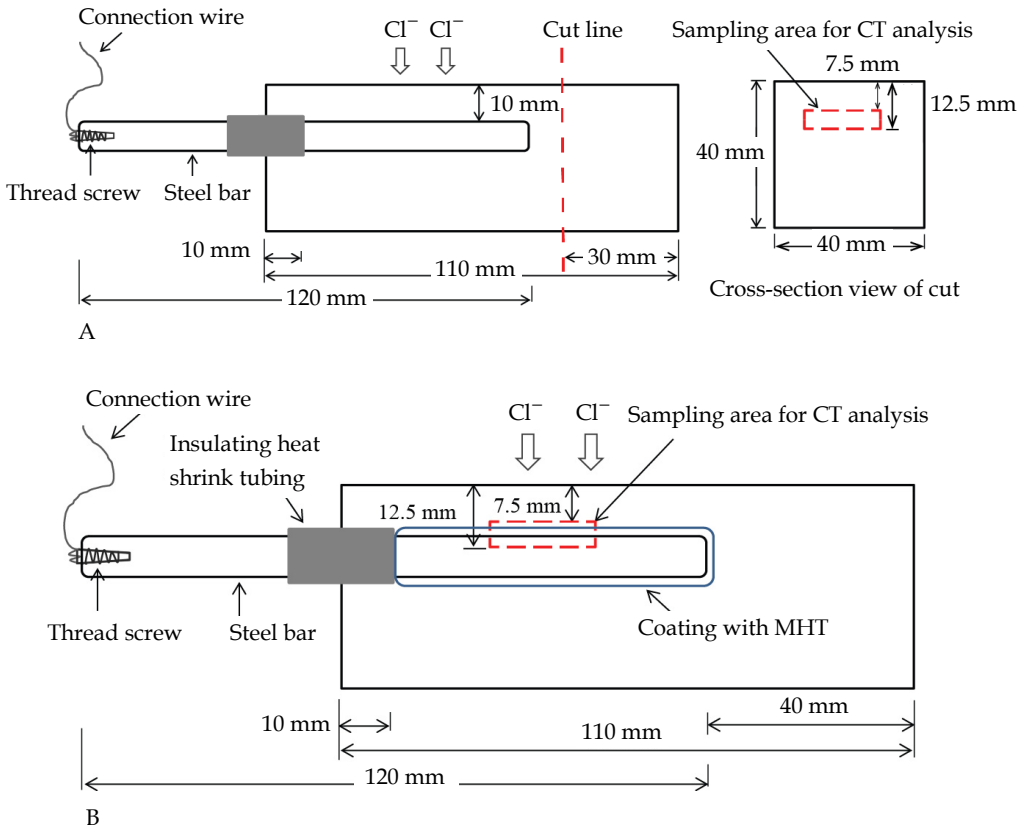

Figure 5. Schematic illustration of sampling areas for chloride threshold (CT) analysis in mortar prism with an embedded steel bar: (A) MHT incorporated in the bulk mortar; (B) MHT incorporated in the coating on the rebar.

including nitric acid dissolution, described elsewhere (Yang et al. 2015). The cement content was calculated according to recommended methods (Castellote and Andrade 2001) by subtracting the weight of insoluble matter from the initial weight of the oven-dried mortar powder and correcting for hydration water, assuming 18% of the acid soluble cementitious mass was hydration water in addition to subtraction of the weight of MHTs from the total acid soluble mass.

3 Results and discussion

3.1 Chloride exchange in simulated concrete pore solution

The chloride exchange properties of the two MHTs were investigated in 0.1 M NaOH solution containing chloride ions. After the predetermined exchange time from 2-120 h, the MHT solid was separated from the bulk solution. The amount of chlorides in the remaining MHT solid and the amount of released inhibitors in the supernatant were subsequently analyzed. The chloride exchange and inhibitor release ratios (in molar fraction) were calculated according to the following equations (Eqs. 3 and 4):

$$\text{Chloride exchange ratio} = \frac{m_b/M_{cl}}{m_{MHT}W_{Inh}/M_{Inh}}100\% \quad (3)$$

$$\text{Inhibitor release ratio} = \frac{m_{Inh}/M_{Inh}}{m_{MHT}W_{Inh}/M_{Inh}} = \frac{m_{Inh}}{m_{MHT}W_{Inh}}100\% \quad (4)$$

where m_b (g) is the mass of bound chloride detected in the remaining solid MHT; m_{MHT} (g) is the mass of dry solid MHT (i.e. MHT-pAB, or MHT-NO_2); M_{cl} (g/mol) is the molecular weight of chloride (i.e., 35.5); W_{Inh} (%) is the original percentage content of the intercalated inhibitive anion by mass of MHT (i.e., 11% NO_2- and 32% -pAB); M_{Inh} (g/mol) is the molecular weight of the intercalated inhibitive anion (136 for -pAB, and 46 for -NO_2); m_{Inh} (g) is the mass of the released inhibitive anion detected in the supernatant (i.e., -pAB, or -NO_2).

The profiles of chloride bound by MHT and corresponding inhibitors released from MHT are given in Figure 6, in which the chloride exchange and inhibitor release ratios were plotted against the exchange time. XRD was employed to qualitatively analyze the crystal structure of MHT before and after the chloride exchange experiments to further confirm the occurrence of ion exchange between the intercalated inhibitive anions in MHT and free chlorides in simulated concrete pore solution. The relevant XRD patterns are shown in Figure 7.

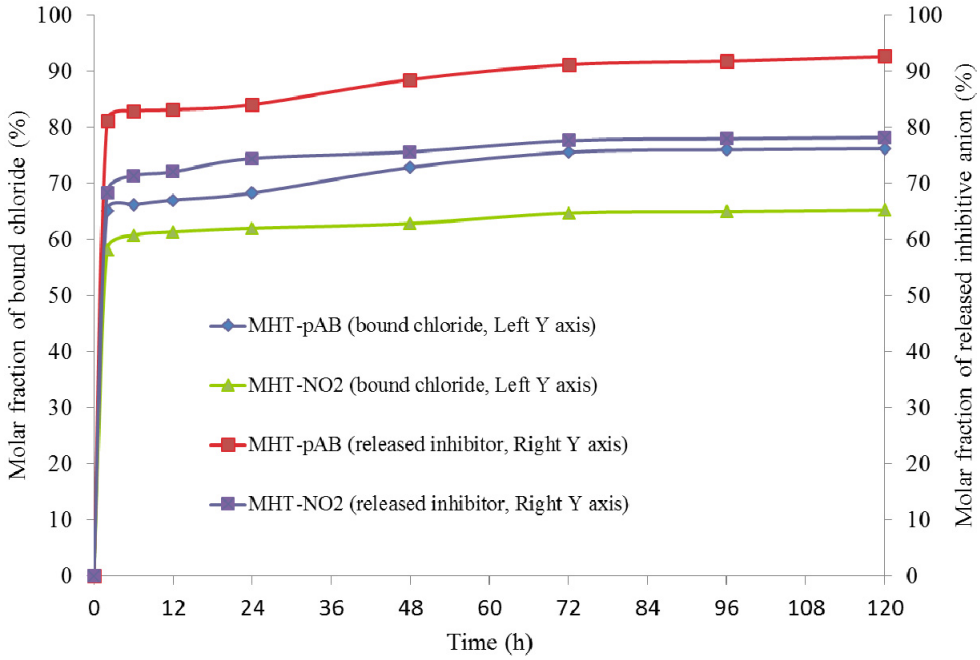

Figure 6. Chloride binding and inhibitor release profiles of the two synthesized MHTs

As can be seen from Figure 6, both MHTs show a rapid increase of concentration of the bound chloride and the released inhibitor during the first 2 h followed by a slow and more sustained exchange until a period time of 120 h. The similarity of the two profiles proves the occurrence of ion exchange of the intercalated inhibitive ions (i.e., -pAB, or $-NO_2$) with the chlorides. It is interesting to find that the inhibitor release ratios of MHTs are higher than their corresponding bound chloride ratios. For example, the bound chloride ratio at 120 h was 76% for MHT-pAB, and 65% for MHT-NO_2, whilst their corresponding inhibitor release ratio at 120 h was 93% and 78%. There may be a number of explanations for this phenomenon.

The differences between these inhibitor release and bound chloride ratios may be caused by the co-existence of competitive OH- ions or by the exchange of intercalated inhibitive ions by CO_3^{2-}, which could originate from reaction of airborne CO_2 with the highly alkaline solution. Since the fact that the MHTs were synthesized in alkaline solution (pH is around 10) over a reaction time of 24 h, the OH- may not be expected to exchange the intercalated inhibitors from MHT. However, previous research (You et al. 2001, bin Hussein et al 2002, Hang et al 2012) reported the possibility of decrease of MHT in a solution with very high

alkalinity (pH 13-14), although the effect was limited, due to the adsorption of OH- by hydrotalcite-like compounds. In this research the synthesis of MHT was performed in a solution at pH around 10, and the chloride exchange experiment was conducted in a solution with higher alkalinity (i.e., 0.1M NaOH + 0.5M NaCl; pH is around 13). That is to say, the higher solution alkalinity in the chloride exchange experiment could cause a different OH- "equilibrium" concentration with MHT compared to that in the condition of synthesis, which in turn may result in a partial replacement of inhibitive ions by OH-. In addition, some impurities of the inhibitive anions could be adsorbed on the surface of the

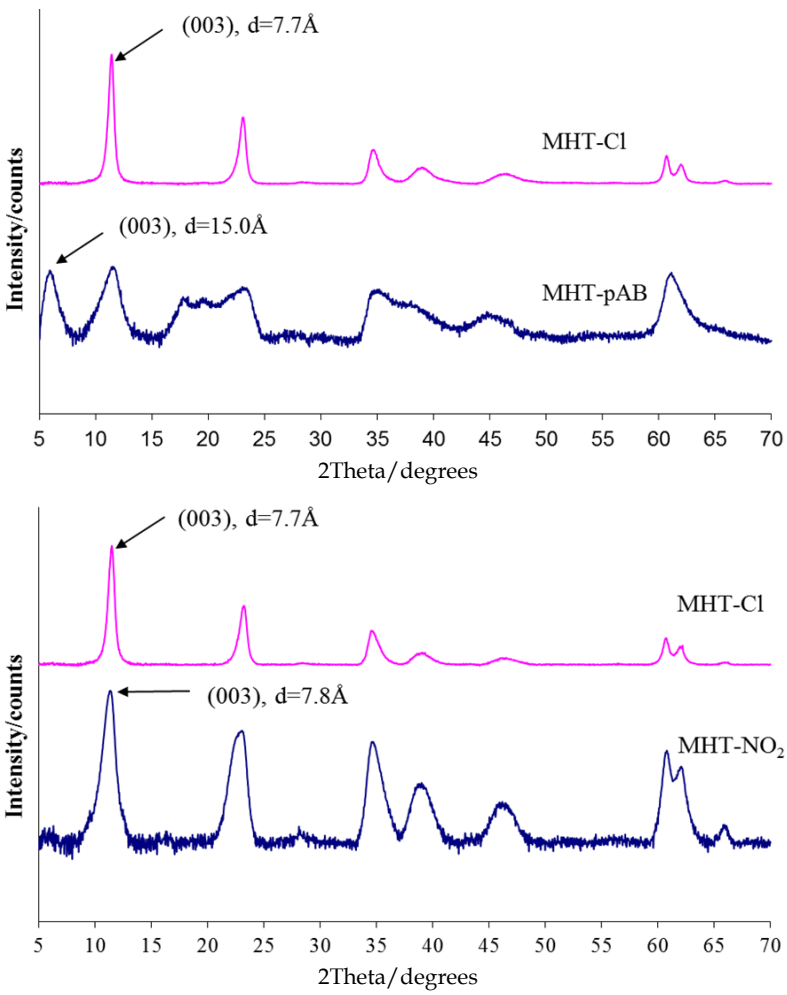

Figure 7. XRD patterns of MHT-pAB (top) and MHT-NO_2 (bottom) before (lower) and after (upper) chloride exchange

MHT crystals due to electrostatic attraction during the synthesis and post-synthesis processes. The liberation of these impurities might be another possibility causing the difference between inhibitor release and bound chloride ratios.

The crystal structure change of the MHTs before and after chloride exchange confirmed the occurrence of ion exchange between chlorides and the interlayer inhibitive anions (i.e. -NO_2, or -pAB). As can be seen from Figure. 7, the characteristic peaks in XRD patterns of MHT-pAB and MHT-NO_2 have been changed after chloride exchange. The d-spacing value of (003) which correlates to the length of interlayer space of MHT was found changed respectively from the original 15.0 Å (MHT-pAB) and 7.8 Å (MHT-NO_2) to 7.7 Å, a value which is in good agreement with reported basal spacing of chloride intercalated hydrotalcites (Bothe and Brown 2004, Thomas et al. 2012, Buchheit 2003). This information clearly reveals that exchange indeed occurred between chloride and the intercalated inhibitive ions in both MHTs. In addition, the sharper and more symmetric diffraction peaks shown in XRD patterns of MHT-Cl suggest a typical layered structure with higher crystallinity resulting from the ion exchange process.

3.2 ***Mortar test***

The OCP (i.e. E_{corr}) evolution of steel bars obtained versus SCE and Titanium reference electrode during the accelerated chloride migration test are shown respectively in Figures 8 and 9, where each value has been averaged from the results of three to four parallel specimens. The time scale of the x-axis in the two figures is the test running time which includes the "power on" time and the "waiting" time (i.e., "power off" time) before depassivation and the continued time after depassivation when the specimens were disconnected from the power. As can be seen from the two figures, the OCP evolution obtained from the two different reference electrodes follows the same trend, which suggests that the use of platinized titanium mesh as a reference electrode is feasible in this research. It is interesting to note that in the later stage of the test, after the specimen was disconnected from the power for several days, the OCPs of all the specimens, except for MHT-NO_2 (10%), started to increase and went on to become more positive than the empirical passive-active "boundary" value of E_{corr} = -350 mV. This may indicate that the steel bars are experiencing repassivation. The i_{corr} evolution obtained by LPR measurements, which are not shown here, further confirmed the observation from the OCP measurements, in particular with regard to the time to corrosion initiation.

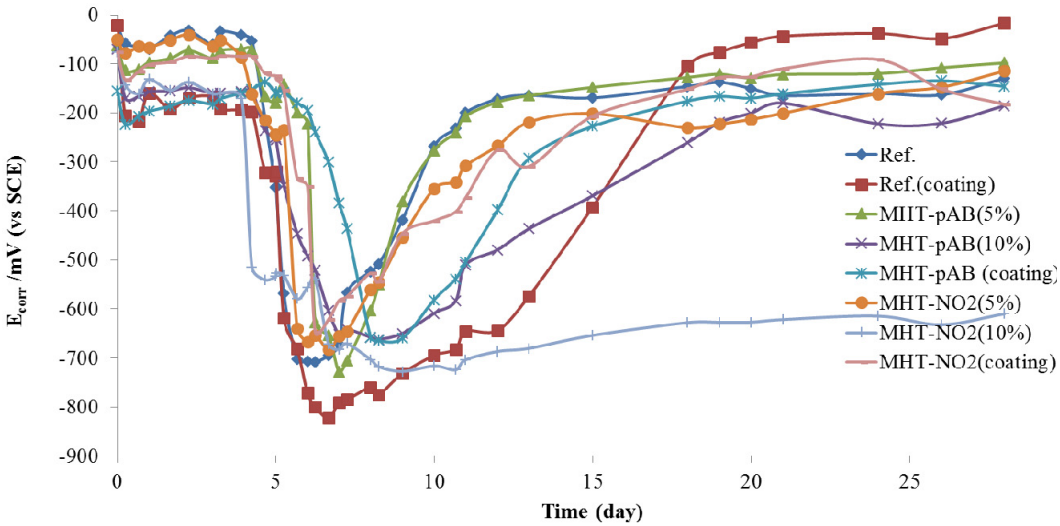

Figure 8. The OCP/ E_{corr} (average of 3-4 specimens) evolution obtained using SCE as reference electrode for rebars embedded in mortar specimens in the accelerated chloride migration test

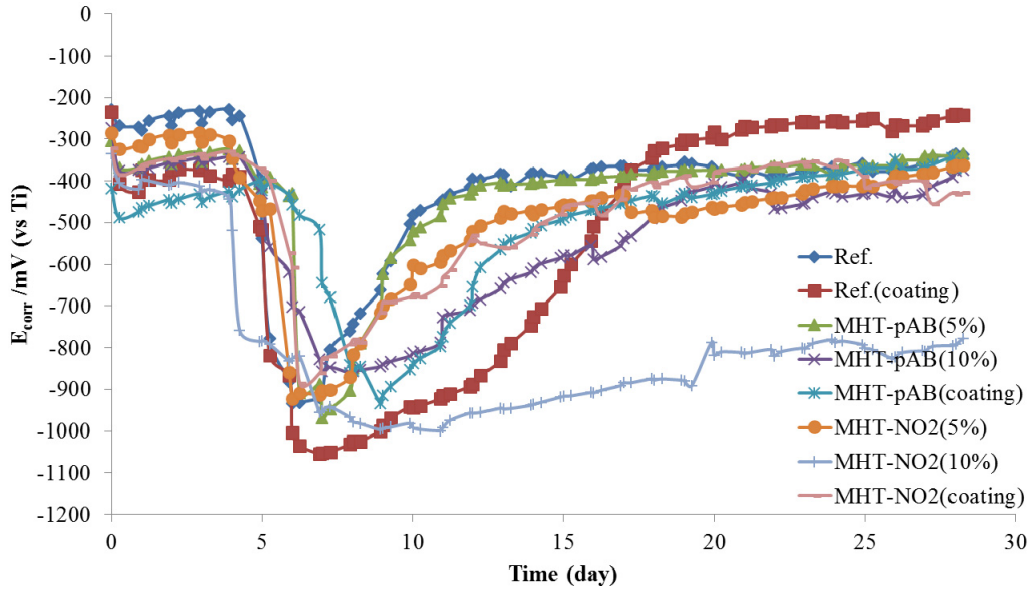

Figure 9. The OCP/ E_{corr} (average of 3-4 specimens) evolution obtained using the platinized titanium mesh as reference electrode for rebars embedded in mortar specimens in the accelerated chloride migration test

The mortar samples were broken after finishing the accelerated migration test and the occurrence of corrosion pits was verified by visual inspection. More and severe corrosion pits were found on the steel bar from MHT-NO_2 (10%) samples which correlates to a longer period of active corrosion as suggested by a negative OCP for a longer time (Figure 9). In most cases, repassivation appeared to occur in 5 to 10 days after the onset of corrosion, indicated by a decrease of i_{corr} after switching off the polarisation. This repassivation is probably due to hydroxyl ions entering pits formed by the strong inflow of chloride ions due to the polarization (migration). Why repassivation did not seem to occur with 10% MHT-NO_2 is not clear. It may have to do with the higher porosity of this particular mix (Yang et al. 2015), with the specific behavior of NO_2- as inhibitor, a combination of both or a yet unknown factor.

Figure 10 shows the representative curves of E_{corr} evolution over the first 120 "power on" testing hours (here the "waiting time" during the test has been subtracted and is not included in the x-axis) during which the depassivation was detected. Table 1 gives the average depassivation time obtained from OCP and LPR measurements and measured chloride threshold values from the accelerated chloride migration test. The chloride threshold (CT) values were averaged from two or three specimens and are expressed as total chloride by mass of cement. As can be seen from Table 1, compared to Ref., MHT-pAB(5%) and MHT-NO_2 (5%) show a relatively longer time-to-depassivation t_d and a higher w/c, while Ref.(coating), which has the same bulk w/c, gave almost the same value. On the other hand, both MHT-pAB (coating) and MHT-NO_2 (coating) showed higher t_d values than Ref. while they have a higher w/c. The chloride transport can be related to the combined effects of the w/c, the amount of cementitious phases as well as the added MHT which are available to react with chloride hindering its ingress. Consequently, these observations support the important role of MHT's active chloride binding capacity in slowing down the chloride ingress. The relatively lower t_d values of the specimens with a higher percentage of MHTs, i.e., MHT-pAB (10%) and MHT-NO_2 (10%) were likely due to a higher chloride migration coefficient resulting from a higher w/c ratio. Mortars with MHT added while increasing the w/c also have a higher porosity as described elsewhere (Yang et al. 2015).

On the other hand, as can be seen from Table 1, compared to the Ref., the CT of MHT specimens was increased to a higher level, being 67%, the highest percentage of increase

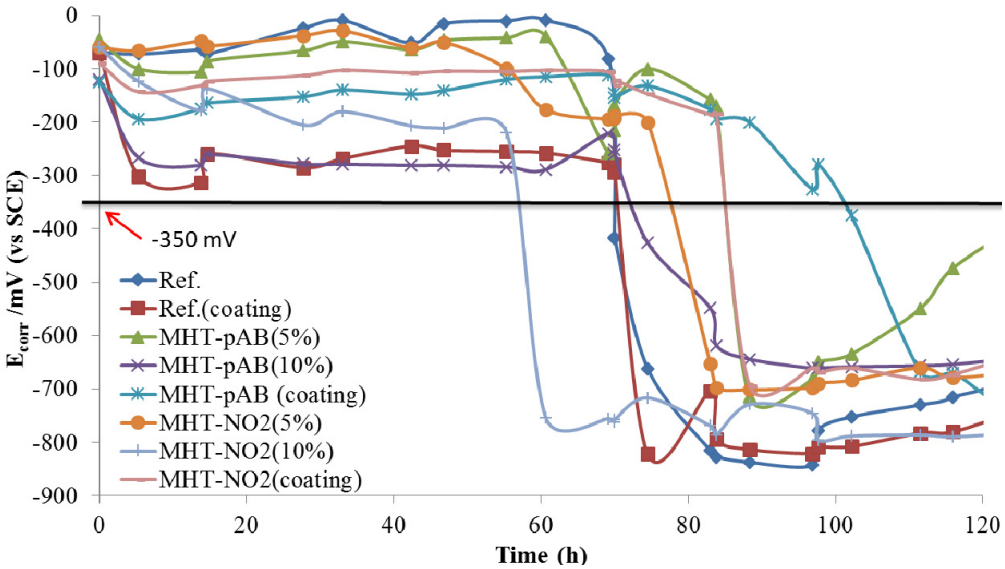

Figure 10. The evolution of E_{corr} /OCP for rebars embedded in mortar specimens during the early stage of the accelerated chloride migration test; the "waiting time/power off" has been deducted and is not included in the time scale of the x-axis.

for MHT-pAB(coating) and 28% the lowest for MHT-NO_2 (5%). Considering the proposed dual function working mechanism of MHT (Buchheit et al 2003, Yang et al. 2013), the increased CT level resulting from the incorporation of MHT could be ascribed to the combined effect of active chloride binding of MHT and the inhibiting effect of the simultaneously released inhibitors. In addition, for MHTs with the same dosage (i.e. 5%, 10% in bulk and 20% in coating), specimens with MHT-pAB exhibited higher CT values than those with MHT-NO_2, likely owing to the higher chloride binding/exchange capacity of the MHT-pAB than MHT-NO_2, as found in the exchange experiments (Figure 6), which in turn resulted in lower amounts of -NO_2 released from MHT compared to -pAB. Therefore, a lower amount of bound chloride as well as a lower amount of released inhibitor in the case of MHT-NO_2 may be responsible for the lower CT values compared to similar specimens with MHT-pAB. Moreover, regardless of the two application ways, a higher mixing percentage of both MHTs, that is to say 10% relative to 5% in mortar and 20% in the coating relative to 10% in mortar, was found to increase the CT as well. In addition to the higher chloride binding capacity resulting from the higher added amount of MHT, the relatively higher concentration of released inhibitors (i.e, -pAB and -NO_2) is

Table 1. The time until depassivation of the reinforcing steel in the accelerated chloride migration test, bulk w/c ratios and chloride threshold (Standard deviation is denoted by ±)

Sample group	Ref.	Ref. (coat.)	MHT-pAB (5%)	MHT-pAB (10%)	MHT-pAB (coat.)	MHT-NO_2 (5%)	MHT-NO_2 (10%)	MHT-NO_2 (coat.)
Depassivation time (h) by OCP	72 ±3	73 ±3	87 ±3	80 ±15	100 ±10	80 ±7	65 ±8	87 ±3
Depassivation time (h) by LPR	80 ±7	78 ±8	101 ±8	78 ±8	118 ±8	90 ±8	84 ±14	92 ±8
w/c (bulk)	0.50	0.50	0.53	0.56	0.50	0.53	0.56	0.50
Chloride threshold (% mass of cement)	0.93 ±0.09	1.00 ±0.11	1.24 ±0.16	1.36 ±0.06	1.55 ±0.16	1.19 ±0.14	1.34 ±0.02	1.44 ±0.03

considered to have contributed to raising the CT level. For the Ref.(coating), in which the rebar was coated with a layer of pure cement paste, the formation of a more dense and cement rich layer at the steel-paste interface relative to the steel-mortar interface of Ref. is believed to be the main reason for the increase of CT (Yonezawa et al. 1998, Glass and Buenfeld 1995), but the increase percentage of CT being 7% (0.93 vs 1.00) is not as high as those of MHT specimens.

4 Conclusions

The ion exchange capability of two MHTs (i.e., MHT-pAB and MHT-NO_2) was first investigated in alkaline chloride solution. The analysis of the chloride binding and inhibitor releasing profiles and XRD characterization of the crystal structure of the two MHTs before and after chloride exchange experiments confirmed that ion exchange between free chloride ions in the alkaline solution and the intercalated anions in MHTs indeed occurred. Then, the two MHTs were incorporated into mortar specimens (with different w/c ratios) with embedded steel in two different ways: (1) as one of the mixing components in bulk mortar; (2) as part of a cement paste coating on the reinforcing steel.

The anti-corrosion performance of the two MHTs was investigated by a modified accelerated chloride migration test. The results revealed that both the incorporation of MHT-pAB to replace 5% cement weight in mortar and MHT (for both MHT-pAB and MHT-NO_2) applied as 20% of a cement paste coating of the reinforcing steel produced a notably extended time to corrosion initiation. This is despite the fact that the mortars with MHT had a higher w/c, which would normally be thought to reduce the time to corrosion initiation (by increasing the chloride diffusion coefficient). The chloride threshold (CT) of MHT specimens, which was expressed as total chloride percentage by mass of cement, was found to increase to a higher level. In addition, it was found that specimens with MHT-pAB exhibited higher CT values than comparable specimens with MHT-NO_2. Considering the effect of increased w/c for mortar with MHT, this interpretation of the effects of MHT is conservative.

In summary, experimental results presented in this paper served to validate the possibilities of MHTs as chloride scavengers and inhibitor release agents to prevent or postpone chloride-induced reinforcement corrosion in concrete structures. An appropriate mixing dosage should be adopted and applied in a proper way, i.e., either incorporation of a small amount (in particular, MHT-pAB at 5% by mass of cement) in the bulk concrete or as part of a cement paste coating of the reinforcing steel (with 20% MHT-pAB or MHT-NO_2 by mass of cement). Regarding these two modes of application, both have their pros and cons. Adding MHT to the bulk of concrete is simple, but requires a relatively high amount of MHT. This could be economically more feasible for relatively thin elements. On the other hand, applying an MHT modified cement paste only to the reinforcement requires much less material (but more labour). However, the cement paste is rather brittle, so bending of reinforcing bars after application of the paste should be avoided and handling should always be aimed at preserving the MHT-cement coating. One possibility is to apply MHT-paste to prefabricated rebar mesh in the production of precast concrete elements. Another option is to spray MHT-cement paste after forming rebar cages in cast in situ projects. Identifying practical and economical options and limitations for application is obviously an area for more research.

Acknowledgements

The research was carried out under project number M81.609337 in the framework of the Research Program of the Materials innovation institute (M2i) (www.m2i.nl). Dr. Hartmut Fischer at TNO Materials Performance is acknowledged for his contribution in previous stages of this project. Sasol Germany GmbH is acknowledged for providing the carbonate hydrotalcite PURAL® MG 63 HT that was used in this work.

References

Alonso, C., Andrade, C., Castellote, M., Castro, P. (2000). Chloride threshold values to depassivate reinforcing bars embedded in a standardized OPC mortar, *Cement and Concrete Research*, 30(7): 1047-1055.

Andrade, C., Buják, R. (2013). Effects of some mineral additions to Portland cement on reinforcement corrosion, *Cement and Concrete Research*, 53:59-67.

Andrade, C., Gonzalez, J. (1978). Quantitative measurements of corrosion rate of reinforcing steels embedded in concrete using polarization resistance measurements, *Materials and Corrosion*, 29: 515-519.

Andrade, C., Rebolledo, N. (2012) Accelerated evaluation of corrosion inhibition by means of the integral corrosion test, *International Conference on Concrete Repair, Rehabilitation and Retrofitting III*, Cape Town, South Africa, CRC Press, pp. 364-368.

Arya, C., Xu, Y. (1995). Effect of cement type on chloride binding and corrosion of steel in concrete. *Cement and Concrete Research*, 25(4):893-902.

Baweja, D., Roper, H., Sirivivatnanon, V. (1993). Relationships between anodic polarisation and corrosion of steel in concrete, Cement and Concrete Research, 23:1418-1430.

Bertolini, L., Elsener, B., Pedeferri, P., Redaelli, E., Polder, R. 2013. *Corrosion of Steel in Concrete: Prevention, Diagnosis, Repair*. 2nd Ed. Weinheim: Wiley-VCH.

bin Hussein MZ, Zainal Z, Yahaya AH, Foo DWV. (2002). Controlled release of a plant growth regulator, α-naphthaleneacetate from the lamella of Zn–Al-layered double hydroxide nanocomposite. *Journal of Controlled Release*, 82(2):417-27.

Bothe Jr JV, Brown PW. (2004). PhreeqC modeling of Friedel's salt equilibria at 23±1 °C. *Cement and Concrete Research*, 34(6):1057-63.

Buchheit RG, Guan H, Mahajanam S, Wong F. (2003). Active corrosion protection and corrosion sensing in chromate-free organic coatings. *Progress in Organic Coatings*, 47(3):174-82.

Castellote, M., Andrade, C. (2001). Round-Robin test on chloride analysis in concrete—Part I: Analysis of total chloride content, *Materials and Structures*, 34 (9): 532-549.

Castellote, M., Andrade, C., Alonso, C. (2002). Accelerated simultaneous determination of the chloride depassivation threshold and of the non-stationary diffusion coefficient values, *Corrosion Science*, 44 (11): 2409-2424.

Cigna, R., Andrade, C., Nürnberger, U., Polder, R. Weydert R. and E. Seitz (Eds.) 2002. COST 521: Final Report. Luxembourg.

Dhir, R.K., El-Mohr, M. A. K. and Dyer, T.D. (1996). Chloride binding in GGBS concrete. *Cement and Concrete Research*, 26(12):1767-1773.

Elsener, B. 2001. Corrosion Inhibitors for Steel in Concrete-State of the Art Report. EFC Publication No. 35, London: IOM Communications.

Elsener, B., Addari, D., Coray, S. and Rossi, A. (2010). Stainless Steel Reinforcing Bars-Reason for Their High Pitting Corrosion Resistance. *Materials and Corrosion*, 61:1-9.

Glass, G. K., Buenfeld, N. R. (2000). The influence of chloride binding on the chloride induced corrosion risk in reinforced concrete. *Corrosion Science*, 42(2):329-344.

Glass, G. K., Buenfeld, N. R. Chloride threshold levels for corrosion induced deterioration of steel. In: Nilsson L, Ollivier J, editors. 1st RILEM International Workshop on Chloride Penetration into Concrete: Rilem Publications SARL; 1995. p. 429-40.

Hang, T.T.X., Truc, T.A., Duong, N.T., Vu, P.G., Hoang, T. (2012). Preparation and characterization of nanocontainers of corrosion inhibitor based on layered double hydroxides. *Applied Clay Science*, 67:18-25.

Kayali, O., Khan, M.S.H, Ahmed, M.S. (2012). The role of hydrotalcite in chloride binding and corrosion protection in concretes with ground granulated blast furnace slag. Cement and. *Concrete Composites*, 34(8):936-945.

Page, C., Short, N, El Tarras, A. (1981). Diffusion of chloride ions in hardened cement pastes. *Cement and Concrete Research*, 11(3):395-406.

Pedeferri, P. 1996. Cathodic Protection and Cathodic Prevention. *Construction and Building Materials*, 10(5), 391-402.

Polder, R., Peelen, W.H.A. (2002). Characterisation of chloride transport and reinforcement corrosion in concrete under cyclic wetting and drying by electrical resistivity. *Cement and Concrete Composites*, 24(5):427-435.

Polder, R.B., Pan, Y., Courage, W., Peelen, W.H.A. (2016). Preliminary study of life cycle cost of preventive measures and repair options for corrosion in concrete infrastructure, *HERON*, 61:1-14.

Polder, R.B., Peelen, W.H.A., Courage, W.M.G. (2012). Non-traditional assessment and maintenance methods for aging concrete structures - Technical and non-technical issues, *Materials and Corrosion*, 63 (12):1147-1153.

Poursaee, A., Hansson, C. (2007). Reinforcing steel passivation in mortar and pore solution, *Cement and Concrete Research*, 37 (7): 1127-1133.

Thomas, M., Hooton, R., Scott, A., Zibara, H. (2012). The effect of supplementary cementitious materials on chloride binding in hardened cement paste. *Cement and Concrete Research*, 42(1):1-7.

Tuutti, K. 1982. *Corrosion of steel in concrete*. Stockholm: Swedish foundation for concrete research (CBI).

Yang, Z. *Modified Hydrotalcites as Smart Additives for Improved Corrosion Protection of Reinforced Concrete*. Ph.D. thesis, Delft University of Technology, the Netherlands, 2015.

Yang, Z., Fischer, H., Polder, R. (2013). Modified hydrotalcites as a new emerging class of smart additive of reinforced concrete for anti-corrosion applications: a literature review. *Materials and Corrosion*, 64(12):1066-74.

Yang, Z., Fischer, H., Polder, R. (2014). Synthesis and characterisation of modified hydrotalcites and their ion exchange characteristics in chloride-rich simulated concrete pore solution. *Cement and Concrete Composites*, 47:87-93.

Yang, Z., Fischer, H., Polder, R. (2015). Laboratory investigation of the influence of two types of modified hydrotalcites on chloride ingress into cement mortar, *Cement and Concrete Composites*, 58: 105-113.

Yang, Z., Shi, X., Creighton, A. T. and Peterson, M. M. (2009). Effect of styrene-butadiene rubber latex on the chloride permeability and microstructure of Portland cement mortars. *Construction and Building Materials*, 23(6):2283-2290.

Yonezawa, T., Ashworth, V., Procter, R. (1988). Pore solution composition and chloride effects on the corrosion of steel in concrete. *Corrosion*. 44(7):489-99.

You, Y., Vance, G.F., Zhao, H. (2001). Selenium adsorption on Mg–Al and Zn–Al layered double hydroxides. *Applied Clay Science*, 20(1):13-25.